INTERNATIONAL JOURNAL FOR NUMERICAL METHODS IN FLUIDS, VOL. 8, 165–179 (1988)

UNSTEADY BOUNDARY LAYER AND ITS SEPARATION OVER A HEATED CIRCULAR CYLINDER

JAE-SOO KIM AND KEUN-SHIK CHANG

Department of Mechanical Engineering, Korea Advanced Institute of Science and Technology, P.O. Box 150, Cheongryang, Seoul, Korea

SUMMARY

A numerical method is developed to solve the coupled unsteady laminar momentum and thermal boundary layers over a circular cylinder impulsively started from rest. The present non-iterative finite difference method, which requires relatively fewer grid points in the reversed flow region than any other method, can easily handle the separating boundary layer flows. The results indicate that the present method has accuracy comparable with the earlier methods, while consuming computer time approximately one order of magnitude less.

The present numerical method allowed investigation of the effect of buoyancy parameter on the starting boundary layer. The time-dependent behaviour of the boundary layer is studied in terms of the appearance of the singularity, the distribution of skin friction and wall heat flux, and the wall position of the inflection point of the velocity profile. The transient as well as buoyancy-dependent patterns of the streamlines and isotherms are also studied.

KEY WORDS Unsteady laminar boundary layer Buoyancy effect Non-iterative finite difference method Boundary layer singularity Separated flow region

INTRODUCTION

Unsteady viscous flows are an important area of fluid mechanics, having a myriad of applications in nature and technology which cannot all be elaborated here. Unsteady phenomena are involved in such flow problems as impulsive starting, periodic body oscillations, moving wall problems, vortex shedding and so on. These problems cannot, in general, be predicted or explained realistically by a potential theory or quasi-steady viscous flow models. Instead, the unsteady boundary layer or Navier–Stokes equations have to be solved directly.

In the present paper, we consider the unsteady boundary layer being developed around a heated circular cylinder impulsively started from rest. The effect of buoyancy on unsteady separation, which has not been properly studied in the literature, is studied parametrically here. A similar flow without the thermal effect was calculated earlier by Telionis and Tsahalis[1] by using a finite difference technique. Their result showed numerical instability when the non-dimensional time τ was 0·65 at a pheripheral station $\theta = 140°$, which was measured from the front stagnation point of the circular cylinder. On the contrary, Cebeci[2] first failed to observe any numerical instability up to $\tau \leqslant 1{\cdot}0$ and found that the solution was smooth. From this result, he suggested that the solution of the boundary layer equations remained smooth for all finite times, even though the boundary layer thickness increased exponentially with time towards the rear stagnation point. In 1982 Van Dommelem and Shen[3] found numerically spontaneous generation of a 'singularity' at time $\tau = 1{\cdot}50$

0271-2091/88/020165-15$07.50

Received 14 October 1986
Revised 18 March 1987

and $\theta = 111{\cdot}0$ using Lagrangian boundary layer co-ordinates. Later, Cebeci[4] extended his computation to times greater than unity and confirmed the development of a hump of large gradient in the displacement thickness at $\tau = 1{\cdot}375$. From this result, he concluded that the computed δ^* distribution suggested a singularity was developing in δ^*. Wang[5] reported also that this singularity appeared at $\tau = 1{\cdot}4$. A similar phenomenon will be examined later in the present paper.

Here, an efficient non-iterative finite difference method is devised for the coupled unsteady momentum and thermal boundary layer equations in Eulerian co-ordinates, which constitutes another objective of the present research. Most of the earlier numerical methods have been iterative. Furthermore, they need hundreds of mesh points in the transverse direction, because the boundary layer thickness grows exponentially with time in the region of reversed flow. Linearizing the general non-linear finite difference equations without losing the formal order of accuracy, we obtained numerical solution non-iteratively at each time step. The technique was first applied to the compressible Navier–Stokes equations by Beam and Warming[6] and then extended to the boundary layer equations by Orlandi and Ferziger[7] and Kim and Chang.[8,9] To reduce the excessive number of grid points necessary in the region of reversed flow, transformed variables similar to those used in the unsteady rear stagnation point flow[10] are utilized in the present formulation, by which the thickness of the computational boundary layer is kept almost constant. The transformed equations are first written as a system of five first-order partial differential equations before they are discretized and linearized. The resultant five implicit finite difference equations, which yield a 5×5 block tridiagonal coefficient matrix when assembled, are readily solved by using a well-known block elimination method. Details of the method are elaborated in the following.

GOVERNING EQUATIONS AND TRANSFORMATIONS

The Boussinesq as well as the boundary layer approximations are adopted in the equations. In the momentum boundary layer, the pressure and the buoyancy force are equally important as a flow-driving agent. The incident main flow is considered to be uniformly upward before it is disturbed by the presence of the heated cylinder. Merkin[10] previously considered a similar flow domain, but it was in a steady state. The non-dimensional governing equations can be written as follows:

$$\frac{\partial u}{\partial x} + \frac{\partial v}{\partial y} = 0, \tag{1}$$

$$\frac{\partial u}{\partial t} + u\frac{\partial u}{\partial x} + v\frac{\partial u}{\partial y} = U_e\frac{\partial U_e}{\partial x} + \frac{Gr}{Re^2}(T - T_\infty)\sin(\pi x) + \frac{\partial^2 u}{\partial y^2}, \tag{2}$$

$$\frac{\partial T}{\partial t} + u\frac{\partial T}{\partial x} + v\frac{\partial T}{\partial y} = \frac{1}{Pr}\frac{\partial^2 T}{\partial y^2}. \tag{3}$$

Boundary conditions are

$$y = 0, \quad u = 0, \quad v = 0, \quad T = T_w,$$

$$y \to \infty, \quad u \to U_e, \quad T \to T_\infty.$$

Because of the various different phases in the growth of the boundary layer and the reversed flow region, we need to switch independent variables from one type to another depending on the elapsed time and characteristic flow regions under development. In order to avoid the singularity associated with impulsive starting, we recommend the transformation in Cebeci[2] as an appropriate

initial form:

$$t = t, \quad x = x, \quad \eta = (1/\sqrt{t})y, \tag{4a}$$

$$\psi = \sqrt{t}U_e f(t, x, \eta), \quad g(t, x, \eta) = (T - T_\infty)/(T_w - T_\infty), \tag{4b}$$

with

$$u = \partial\psi/\partial y, \quad v = -\partial\psi/\partial x. \tag{5}$$

The three differential equations (1)–(3) can be reduced to two expressions of increased order (prime denotes differentiation with respect to η) as

$$f''' + t\frac{\partial U_e}{\partial x}(ff'' - f'^2 + 1) + \frac{\eta}{2}f'' + \frac{t}{U_e}\sin(\pi x)\alpha g = t\frac{\partial f'}{\partial t} + tU_e\left(f'\frac{\partial f'}{\partial x} - f''\frac{\partial f}{\partial x}\right), \tag{6}$$

$$\frac{1}{Pr}g'' + t\frac{\partial U_e}{\partial x}fg' + \frac{\eta}{2}g' = t\frac{\partial g}{\partial t} + tU_e\left(f'\frac{\partial g}{\partial x} - g'\frac{\partial f}{\partial x}\right). \tag{7}$$

Boundary conditions are

$$\eta = 0, \quad f = 0, \quad f' = 0, \quad g = 1,$$

$$\eta \to \infty, \quad f' \to 1, \quad g \to 0.$$

These transformed variables should be used in the time interval $0 \leqslant t \leqslant t_1$, during which the boundary layer is rapidly developed after starting. For $t_1 \leqslant t \leqslant t_2$, the next type of dimensionless variables are appropriate:[2]

$$t = t, \quad x = x, \quad \eta = y, \tag{8a}$$

$$\psi = U_e f(t, x, \eta), \quad g(t, x, \eta) = (T - T_\infty)/(T_w - T_\infty). \tag{8b}$$

Equations (1)–(3) are transformed accordingly as

$$f''' + \frac{\partial U_e}{\partial x}(ff'' - f'^2 + 1) + \frac{\alpha}{U_e}\sin(\pi x)g = \frac{\partial f'}{\partial t} + U_e\left(f'\frac{\partial f'}{\partial x} - f''\frac{\partial f}{\partial x}\right), \tag{9}$$

$$\frac{1}{Pr}g'' + \frac{\partial U_e}{\partial x}fg' = \frac{\partial g}{\partial t} + U_e\left(f'\frac{\partial g}{\partial x} - g'\frac{\partial f}{\partial x}\right). \tag{10}$$

These variables are employed in the entire range of x for the time up to $t = t_2$, during which the rate of boundary layer growth is relatively retarded and the boundary layer thickness is not so large near the rear stagnation point. For $t > t_2$, the second type of transformed variables, as in equation (8), are still valid in $0 < x < x_1$. However, they are switched to a third type of variables in the region $x_1 < x < 1{\cdot}0$. The last transformation, which is extended from the work of Robins and Howarth,[10] designed to treat the rear stagnation point flow, is now applied to the entire boundary layer in the rear part of the circular cylinder containing the reversed flow region:

$$t = t, \quad x = x, \quad \eta = e^{-t}y, \tag{11a}$$

$$\psi = U_e e^{-t} f(t, x, \eta), \quad g(t, x, \eta) = (T - T_\infty)/(T_w - T_\infty). \tag{11b}$$

Equations (9) and (10) are now transformed as

$$f''' + e^{2t}\frac{\partial U_e}{\partial x}(ff'' - f'^2 + 1) + e^{2t}\eta f'' + \frac{\alpha\sin(\pi x)}{U_e}e^{2t}g$$

$$= e^{2t}\frac{\partial f'}{\partial t} + e^{2t}U_e\left(f'\frac{\partial f'}{\partial x} - f''\frac{\partial f}{\partial x}\right), \tag{12}$$

$$\frac{1}{Pr}g'' + e^{2t}\frac{\partial U_e}{\partial x}fg' + e^{2t}\eta g' = e^{2t}\frac{\partial g}{\partial t} + e^{2t}U_e\left(f'\frac{\partial g}{\partial x} - g'\frac{\partial f}{\partial x}\right). \tag{13}$$

Boundary conditions for the second and third type of transformations are the same as those used in the first transformation.

The instants t_1 and t_2 and the station x_1 must be suitably chosen depending on the growth of the boundary layer thickness; and this requires some experience. A basic rule is that one type of transformed variables are kept as long as the thickness of the computational boundary layer remains small in the region of consideration. The time to switch to the next transformation is heralded when the computational boundary layer begins to grow rapidly under one type of transformed variables. The results show practically no change when a small variation is made in the values t_1, t_2 and x_1.

The governing equations are bi-parabolic in the sense that initial condition is required both in time and streamwise direction. The initial data at $t = 0$ are readily obtained from equation (6) and (7) as

$$f''' + \frac{\eta}{2}f'' = 0, \quad \frac{1}{Pr}g'' + \frac{\eta}{2}g' = 0. \tag{14}$$

The exact solutions of these equations are

$$f = \eta\,\mathrm{erf}\left(\frac{\eta}{2}\right) + \frac{2}{\sqrt{\pi}}\left[\exp\left(-\frac{\eta^2}{4}\right) - 1\right],$$

$$f' = \mathrm{erf}\left(\frac{\eta}{2}\right), \quad f'' = \frac{1}{\sqrt{\pi}}\exp\left(-\frac{\eta^2}{4}\right),$$

$$g = \mathrm{erfc}\left(\frac{\eta}{2}\sqrt{(Pr)}\right), \quad g' = -\frac{1}{\sqrt{\pi}}\sqrt{(Pr)}\exp\left(-\frac{\eta^2}{4}Pr\right). \tag{15}$$

At the initial plane $x = 0$, the transformed equations are reduced to a set of mono-parabolic equations, demanding temporal initial data only.

NUMERICAL FORMULATION

The three sets of bi-parabolic equations, (6) and (7), (9) and (10), and (12) and (13), are very similar to one another in thier form. It seems, therefore, sufficient to discuss the solution methodology on a general model of the equations. The order of these differential equations is first reduced by introducing new variables u, v and h (where the symbols u and v are reused with new definitions):

$$f' = u, \tag{16}$$

$$u' = v, \tag{17}$$

$$v' + m_1 fv + m_2 u^2 + m_3 u + m_4 \eta v + m_5 g + m_6 = m_7\frac{\partial u}{\partial t} + m_8\left(u\frac{\partial u}{\partial x} - v\frac{\partial f}{\partial x}\right), \tag{18}$$

$$g' = h, \tag{19}$$

$$\frac{1}{Pr}h + m_1 hf + m_4\eta h = m_7\frac{\partial g}{\partial t} + m_8\left(u\frac{\partial g}{\partial x} - h\frac{\partial f}{\partial x}\right). \tag{20}$$

The boundary conditions are

$$\eta = 0, \quad f = 0, \quad u = 0, \quad g = 1,$$
$$\eta \to \infty, \quad u \to 1, \quad g \to 0.$$

In the above, the general coefficients $m_1, m_2, \ldots, m_8$ are functions of x and t only.

Equations (16)–(20) are solved by advancing the solution in the time co-ordinate while it is marched in the x direction simultaneously. To march in which direction first is unimportant. Discretization in the time direction is made by using an incremental value Δ as

$$W^{n+1} = W^n + \Delta W^{n+1}, \tag{21}$$

where W represents any of the variables f, u, v, g, h or t.

We discretize the time derivatives using a generalized time differencing formula, as first introduced by Beam and Warming:[6]

$$\Delta q^{n+1} = \frac{\phi \Delta t^{n+1}}{1+\zeta}\frac{\partial}{\partial t}(\Delta q^{n+1}) + \frac{\Delta t^{n+1}}{1+\zeta}\frac{\partial q^n}{\partial t} + \frac{\zeta}{1+\zeta}\Delta q^n + O[(\tfrac{1}{2} - \phi + \zeta)(\Delta t^{n+1})^2 + (\Delta t^{n+1})^3], \tag{22}$$

where q represents either the variable v or h. Among the various schemes identifiable by the two parameters $|\zeta| < 1$ and $\phi < 1$, we select a second-order-accurate three-point backward implicit scheme by letting $\zeta = \frac{1}{2}$ and $\phi = 1{\cdot}0$. Introducing equation (22) into equations (18) and (20), we obtain

$$\frac{\Delta t^{n+1}}{1+\zeta}(\phi\, \Delta R^{n+1} + R^n) = \Delta q^{n+1} - \frac{\zeta}{1+\zeta}\Delta q^n + O[(\tfrac{1}{2} - \phi + \zeta)(\Delta t^{n+1})^2 + (\Delta t^{n+1})^3], \tag{23}$$

where R represents the conglomerated terms from equation (18) or (20) equivalent to $\partial q/\partial t$. The non-linear terms contained in the quantity ΔR^{n+1} are now linearized without losing the formal order of accuracy by a similar procedure to that of Kim and Chang.[8]

We now introduce spatial discretization using variable step sizes. Central differencing is done about the point $(i, j-\frac{1}{2})$ for the spatial derivatives in equations (16), (17) and (19) in which the time-like derivatives are not involved any more. For equations (18) and (20), differencing is done either about the point $(i-\frac{1}{2}, j-\frac{1}{2})$ or about the point $(i, j-\frac{1}{2})$, depending on the existence of the reversed flow. In order to consider the effect of backflow, the x derivatives of the incremental values, Δu, Δf and Δg, are discretized by rearward differencing in the reversed flow region. Central differencing is used for the rest of the derivatives in the previous time level. Compared with the method of zig-zag style,[2,3,5] the present method is simple, straightforward and very efficient in treating the reversed flow. The resultant equations are

$$\Delta f_{ij} - \Delta f_{ij-1} - \tfrac{1}{2}\Delta\eta_j(\Delta u_{ij} + \Delta u_{ij-1}) = a_j, \tag{24}$$

$$\Delta u_{ij} - \Delta u_{ij-1} - \tfrac{1}{2}\Delta\eta_j(\Delta v_{ij} + \Delta v_{ij-1}) = b_{j-1}, \tag{25}$$

$$(S_1)_j\Delta v_{ij} + (S_2)_j\Delta v_{ij-1} + (S_3)_j\Delta f_{ij} + (S_4)_j\Delta f_{ij-1} + (S_5)_j\Delta u_{ij} + (S_6)_j\Delta u_{ij-1} + (S_7)_j\Delta g_{ij} + (S_8)_j\Delta g_{ij-1} = C_j, \tag{26}$$

$$\Delta g_{ij} - \Delta g_{ij-1} - \tfrac{1}{2}\Delta\eta_j(\Delta h_{ij} + \Delta h_{ij-1}) = d_{j-1}, \tag{27}$$

$$(P_1)_j\Delta h_{ij} + (P_2)_j\Delta h_{ij-1} + (P_3)_j\Delta f_{ij} + (P_4)_j\Delta f_{ij-1} + (P_5)_j\Delta g_{ij} + (P_6)_j\Delta g_{ij-1} + (P_7)_j\Delta u_{ij} + (P_8)_j\Delta u_{ij-1} + (P_9)_j\Delta v_{ij} + (P_{10})_j\Delta v_{ij-1} = e_j, \tag{28}$$

where the a, b, c, d, e, S and P are functions of known status or the linear coefficients relying on the previous time step only. The above system of equations yields a 5×5 block tridiagonal coefficient matrix when assembled, which is inverted without difficulty by using the well-known block elimination method.

In this computation, the step size is taken as $\Delta x = 0{\cdot}025$, $\Delta t = 0{\cdot}05$ and $\Delta\eta = 0{\cdot}0001$–$1{\cdot}5$ (variable step sizes). The step size in the η direction is varied exponentially. Though the boundary layer thickness is exponentially increasing with time in the rear reversed flow region, the maximum η value remains almost constant by the third type of transformation introduced earlier. We do not need, therefore, to increase the number of grid points in the η direction, and about 50 grid points were sufficient for successful computation.

RESULTS AND DISCUSSION

Flow without buoyancy effect

Many earlier researchers have computed the flow past a circular cylinder impulsively started from rest by using both the Navier–Stokes and boundary layer equations. The results for the unheated circular cylinder are well summarized in Cebeci.[2] Here, we will discuss our results in terms of the wall position of the inflection point of the velocity profile, the time distribution of the displacement thickness and the skin friction, and the appearance of computational instability connected to the boundary layer singularity, one by one. The time required for the reversed flow to appear at the rear stagnation point was $\tau = 0{\cdot}321$. This result agrees very well with other calculations: 0·35 in Reference 1 and 0·320 in Reference 2. The wall position of the inflection point ($f''_w = 0$) of the velocity profile is presented as a function of time in Figure 1, in terms of the buoyancy parameter $\alpha (= Gr/Re^2)$, and is compared with an earlier result. For an unheated cylinder ($\alpha = 0{\cdot}0$), the comparison with Cebeci's result turns out to be very good. Discussion of the results for other values of α will be postponed to the next section. Figure 2 shows the distribution of the dimensionless displacement thickness as a function of θ and τ. It is found that our results are closer to Cebeci[2] than Wang.[5] In Figure 3 the skin friction parameter agrees very well with Cebeci[2], too.

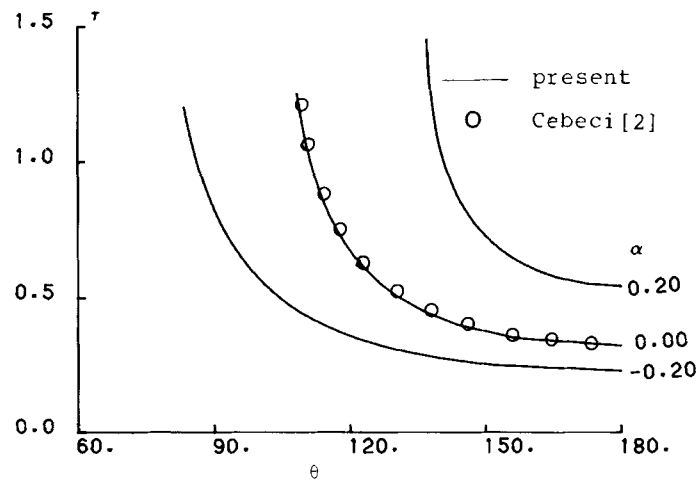

Figure 1. Wall position of the inflection point

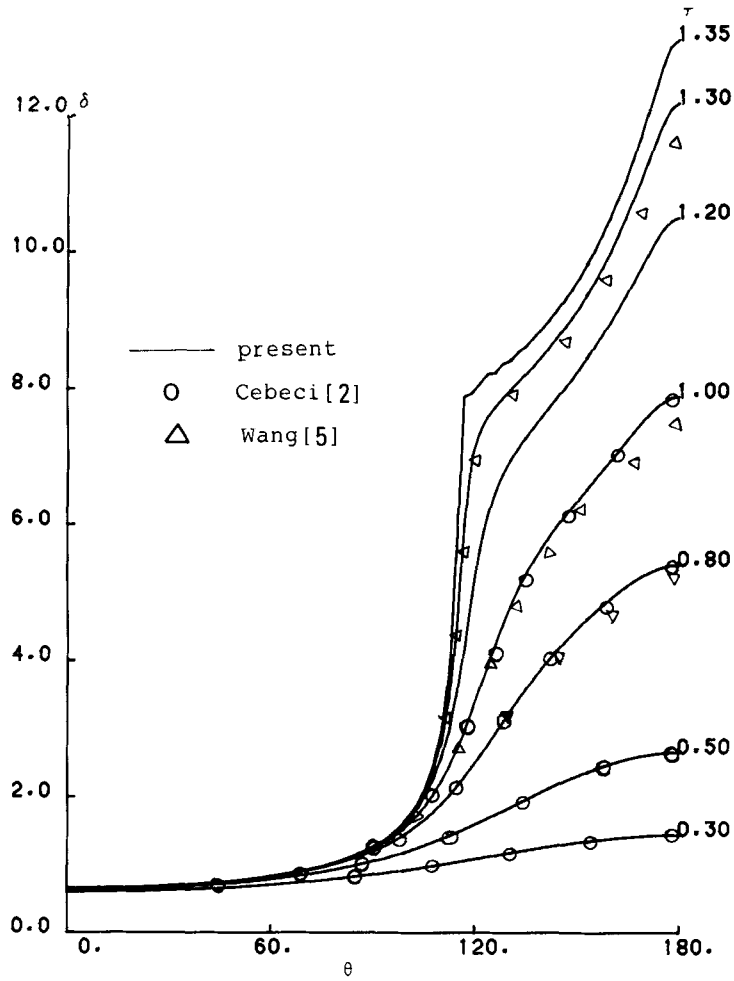

Figure 2. Dimensionless displacement thickness for $\alpha = 0{\cdot}0$

We now discuss the appearance of the boundary layer singularity associated with the unsteady separation. Van Dommelen and Shen[3] found a singularity at $\theta = 111{\cdot}0$ (measured from the forward stagnation point) and at time $\tau = 1{\cdot}50$ in the Lagrangian co-ordinate system. Cebeci[4] stated that the displacement thickness rapidly increased at the position $\theta = 114{\cdot}6$ at time $\tau = 1{\cdot}375$, which was caused by the breakdown of the numerical solution. From this result, he concluded that, while the computed δ distribution for the circular cylinder problem suggested a singularity was developing in δ at $x = 2$, the values of skin friction were smooth and free from any anomalies. Wang[5] showed a similar change in the displacement thickness and defined singularity using the limiting streamline theory. He also argued that, despite the appearance of hump in the flow domain, the skin friction was not immediately influenced by its presence. In Figure 2, the present results for the displacement thickness show a similar hump phenomenon at time $\tau = 1{\cdot}35$. In order to visualize how this 'singularity' develops in the interior of the boundary layer, we plotted the streamline patterns in Figure 4. The left-hand side shows streamlines at various instants. We can see that this numerical instability is first conceived at the centre of the recirculating flow, at the position $\theta = 122{\cdot}0$ and at time $\tau = 1{\cdot}35$, as distinguished by the small sawtooth-type contour.

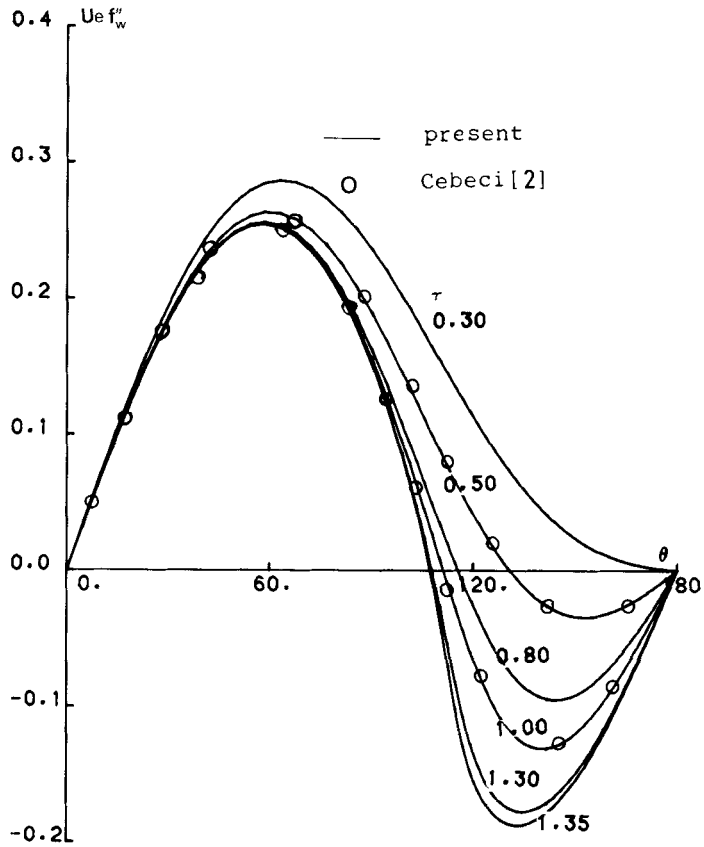

Figure 3. Skin friction parameter for $\alpha = 0{\cdot}0$

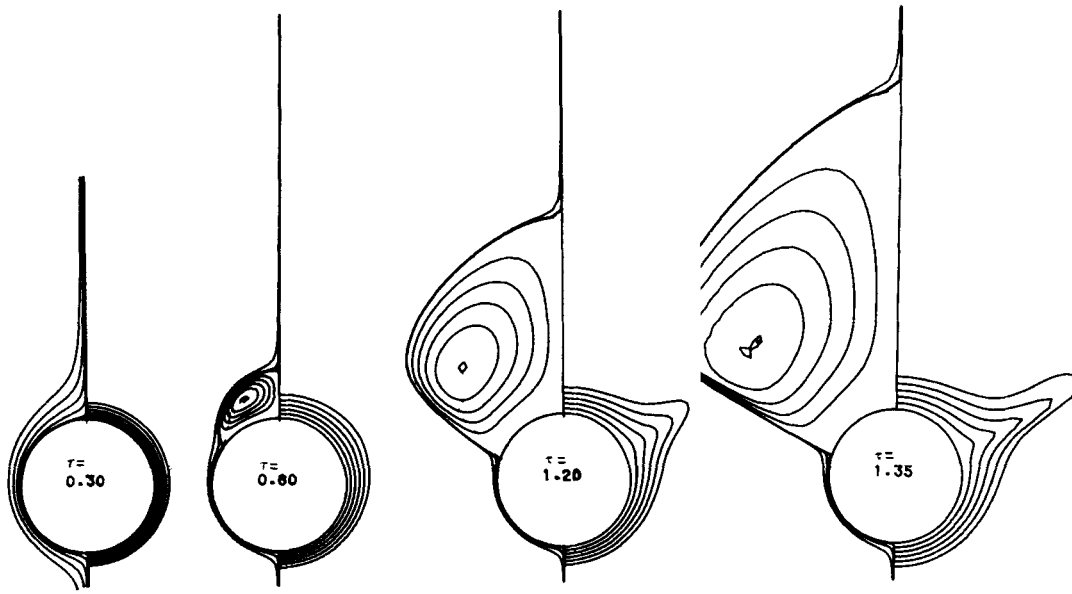

Figure 4. Streamlines and isotherms for $\alpha = 0{\cdot}0$; plotted in the dimensionless (x, y) plane

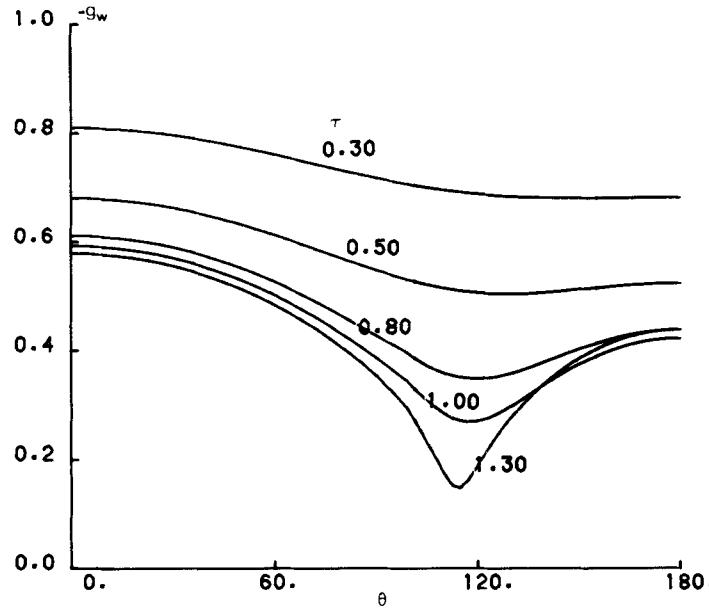

Figure 5. Wall heat flux parameter for $\alpha = 0{\cdot}0$

Numerical results are rapidly broken down subsequently near this point, but the skin friction remains smooth for a while until this instability is propagated to the wall.

The isothermal lines on the right-hand side of Figure 4 show how the thermal boundary layer is developed progressively. The thickness of the thermal boundary layer is largest in the neighbourhood of the point of zero skin friction (but not the stagnation points) and gradually decreases with increasing θ. The reason is that the stream leaves the surface nearly normal to the surface in the neigbourhood of the point of zero skin friction, as can be observed from the streamline pattern. The wall heat flux coefficient decreases monotonically with increasing θ before a reversed flow is encountered, as observed in Figure 5 for large times. The minimum heat flux evidently appears in the neighbourhood of the point of zero skin friction. The reason is obvious again: the temperature gradient falls sharply in that local region due to the flow leaving the cylinder surface. The wall heat flux remains smooth for a while even after the first appearance of the singularity, as was true with the skin friction. In Figures 4 and 10, it is recalled that the radial co-ordinate represents the transformed variable y, not the physical distance.

Flow with buoyancy effect

In Figure 6, our results compare well with those of Merkin[10] for the steady state mixed flow past a heated circular cylinder, for three different values of the buoyancy parameter. A higher buoyancy parameter α means larger skin friction and wall heat flux. The bigger and hotter the circular cylinder is, the higher these flow gradients are, since α is directly proportional to the characteristic length L and the temperature T_c, by definition.

To see the buoyancy effect on the unsteady boundary layer behaviour, we will consider three buoyancy parameters for the time being: $\alpha = -0{\cdot}2, 0{\cdot}0$ and $0{\cdot}2$. Table I shows when and where the singularity first appears for different values of α. It predicts that, for larger α, the θ position and time for the appearance of the singularity are sensitively increased. In Figure 1, where the wall position

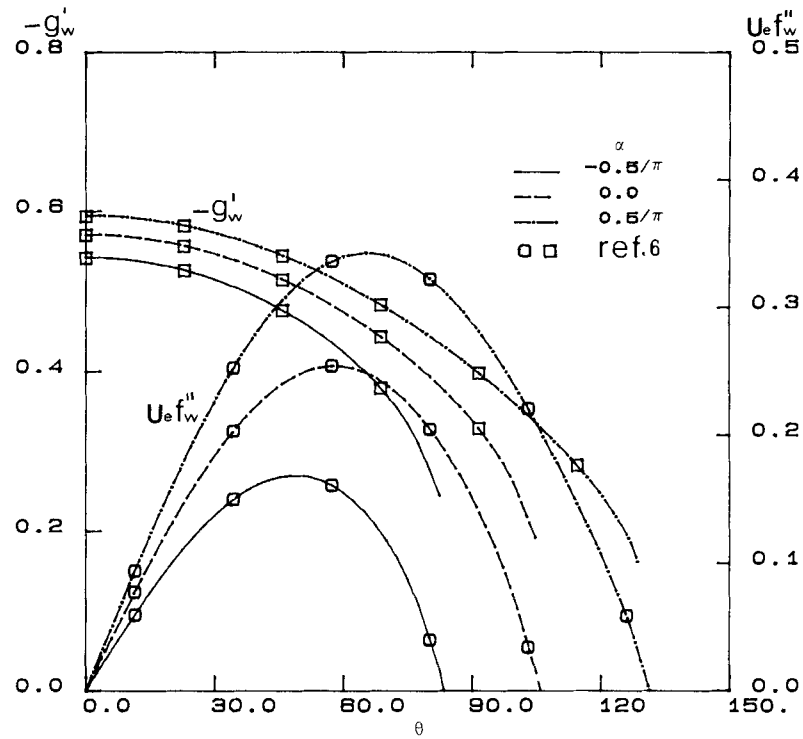

Figure 6. Steady state skin friction and wall heat flux parameters

Table I. Time and position of the singularity

α	−0·2	0	0·2
Time τ(s)	1·125	1·325	1·450
Angle θ(deg)	114	122	144

of the inflection point of the velocity profile is plotted as a function of time, it is observed that the time required for the reversed flow to first appear and the last position of the separation point before a singularity is found in the flow are again strongly affected by the parameter α. This implies that faster convergence to the steady state would be obtained by the higher α (stronger buoyancy) if the boundary layer singularity could be avoided.

In Figure 7, where we have plotted the time-dependent distribution of the displacement thickness, we can judge quantitatively how much thinner the local displacement thickness becomes for $\alpha = 0{\cdot}2$ in comparison with $\alpha = -0{\cdot}2$ at a fixed time and wall position. Figure 8 shows the distribution of the skin friction parameter as a function of α, τ and θ. The skin friction is obviously higher for higher α and is relatively not much changed with time towards the forward part of the circular cylinder. In Figure 9, the heat flux distribution is plotted as a function of α, τ and θ. For more than half of the cylinder surface measured from the forward stagnation point, the heat flux coefficient is smaller for lower α. This trend is reversed, however, toward the rear part of the cylinder. The reason is that the less heated (or less cooled) fluid from the outer region of the boundary layer is impinging downwards toward the rear part of the cylinder on a larger scale for lower α. The streamline pattern given in Figure 10 for three different values of α at the same instant confirms this argument.

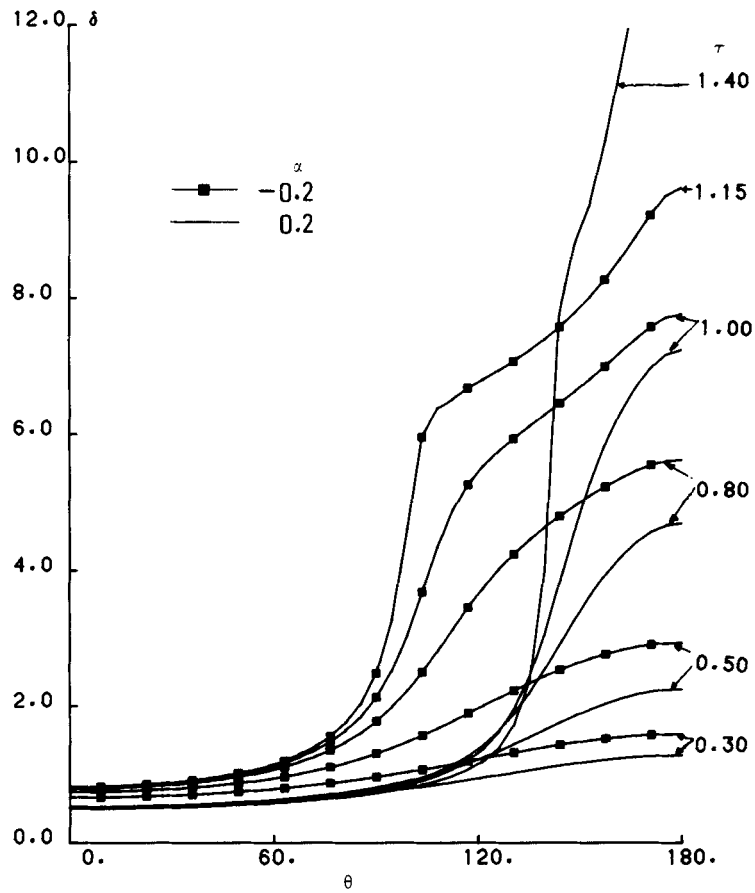

Figure 7. Dimensionless displacement thickness

We have plotted in Figure 11 the time required for the first appearance of the reversed flow (or $f''_w = 0$) at the rear stagnation point of the circular cylinder. This time increases nearly exponentially with the buoyancy parameter α and, at roughly the asymptotic value $\alpha = 0{\cdot}5$, it seems that the wall inflection point is finally heated off. This suggests the important concept that the circular cylinder can be made free from any flow reversal by manipulating the buoyancy parameter.

CONCLUDING REMARKS

A numerical method has been developed to solve the unsteady separated laminar boundary layers with the buoyancy force term included in the momentum equation. Through linearization of the finite difference equations, fast calculation was performed non-iteratively at each time step without losing the formal order of accuracy. It was further possible to treat the reversed flow region with relatively fewer grid points, thanks to the nature of the special co-ordinate transformation adopted or the exponential time dependence in scaling the radial co-ordinate. The consequence is characterized by the computational acceleration by the order of 10 in comparison with other existing methods.

Numerical instability associated with the boundary layer singularity first appeared at the centre

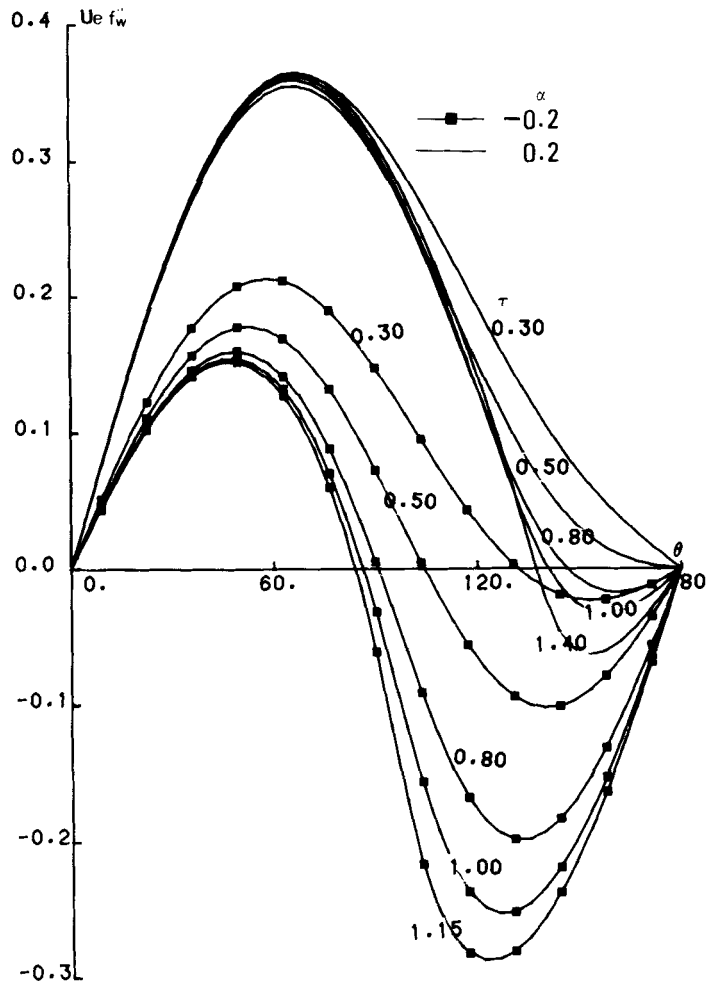

Figure 8. Skin friction parameter

of the recirculating flow behind the heated (or cooled) circular cylinder and then rapidly propagated to other region. The wall skin friction as well as the wall heat flux remained smooth for a while, after the first appearance of the instability, until it reached the surface. The time and position for the first appearance of the singularity were found to be affected sensitively by the buoyancy parameter α.

From the discussion so far, it is evident that the buoyancy force influences drastically the properties of the otherwise forced flow. With increasing values of α, the reversed flow region behind the circular cylinder is reduced in scale and the skin friction is always elevated everywhere, but not the local wall heat flux. At about the asymptotic value $\alpha = 0{\cdot}5$, the circular cylinder finally reaches a state free from any flow reversal.

APPENDIX: NOMENCLATURE

f Dimensionless stream function
g Dimensionless temperature

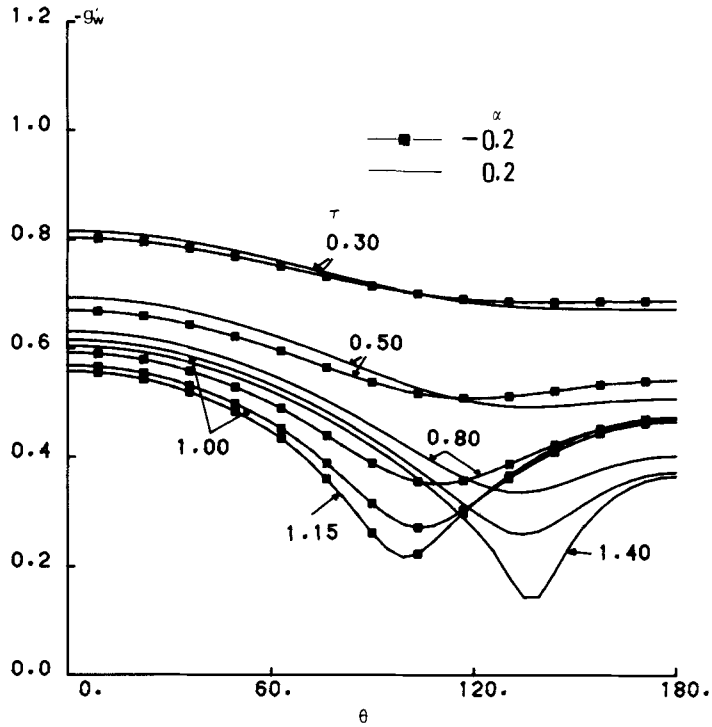

Figure 9. Wall heat flux parameter

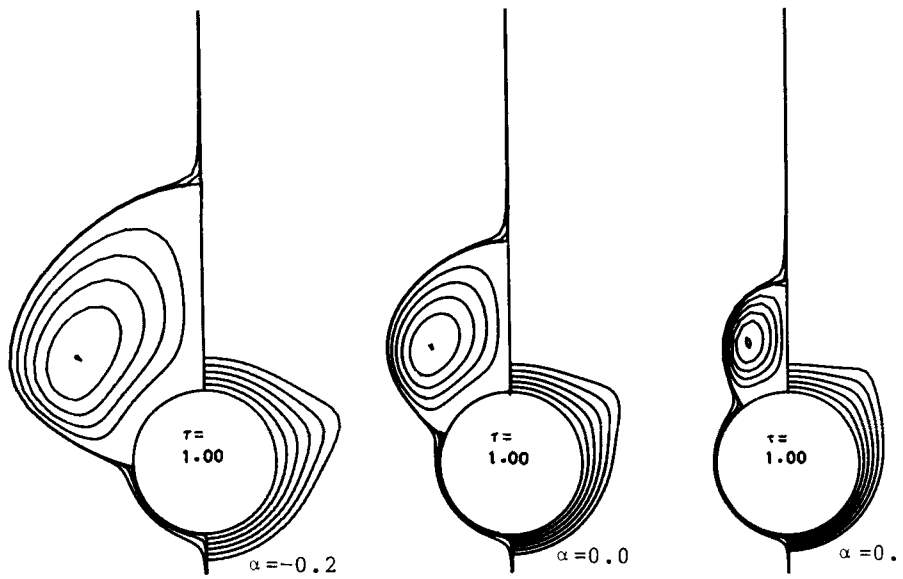

Figure 10. Streamlines and isotherms for $\alpha = 1{\cdot}00$

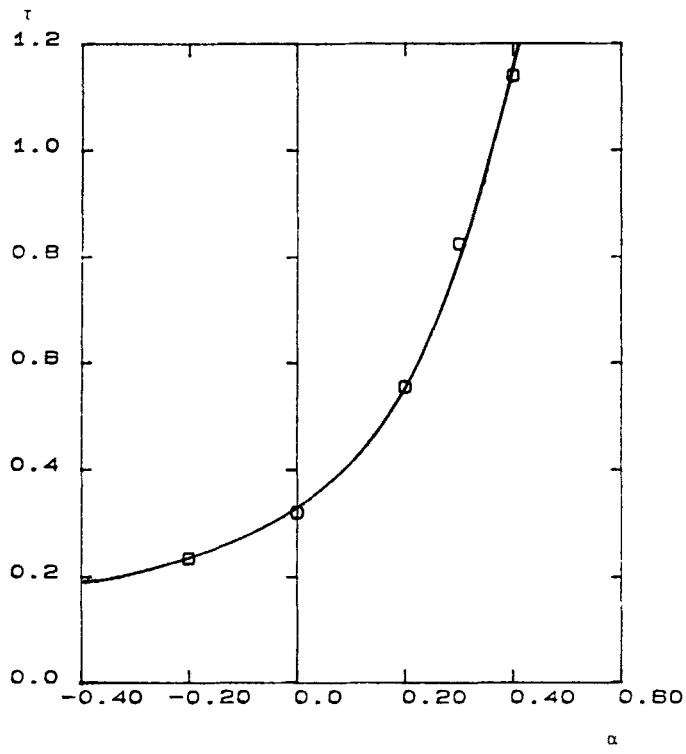

Figure 11. Time required for the first appearance of the reversed flow at the rear stagnation point

Gr	Grashof number
L, V, T_c, t_c	Characteristic length (πR), velocity ($2\pi U^*_\infty$), temperature ($T_w - T^*_\infty$) and time (L/V)
Pr	Prandtl number (= 1·0)
R	Radius of the circular cylinder
Re	Reynolds number
u, v	Dimensionless velocity components in the (x, y) co-ordinates
U_e	Streamwise velocity outside of the boundary layer
x, y	Dimensionless stream co-ordinates ($x = x^*/\pi R, y = y^*\sqrt{Re}/\pi R$)
α	Buoyancy parameter (Gr/Re^2)
η	Dimensionless co-ordinate in the cross-stream direction; see equations (4a), (8a) and (11a)
θ	Azimuthal angle measured from the front stagnation point
τ	Dimensionless time ($t/2$)
δ, δ^*	Dimensionless displacement thickness ($\int_0^\infty (1 - u/U_e)\,dy$)

Superscript

*	Dimensional variables

Subscripts

w	Wall condition
∞	Free stream condition

REFERENCES

1. D. P. Telionis and D. T. Tsahalis, 'Unsteady laminar separation over impulsively moved cylinders', *Acta Astronautica*, **1,** 1487–1505 (1974).
2. T. Cebeci, 'The laminar boundary layer on a circular cylinder started impulsively from rest', *J. Comput. Phys.*, **31,** 153–172 (1979).
3. L. L. Van Dommelen and S. F. Shen, 'The genesis of separation', *Numerical and Physical Aspects of Aerodynamic Flows*, Springer, New York, 1982, pp. 293–311.
4. T. Cebeci, 'Unsteady separation', *Numerical and Physical Aspects of Aerodynamic Flows*, Springer, New York, 1982, pp. 265– 278.
5. K. C. Wang, 'On the current controversy about unsteady separation', *Numerical and Physical Aspects of Aerodynamic Flows*, Springer, New York, 1982, pp. 279–291.
6. R. M. Beam and R. F. Warming, 'An implicit factorized scheme for the compressible Navier–Stokes equations', *AIAA J.*, **16,** 393–402 (1978).
7. P. Orlandi and J. H. Ferziger, 'Implicit noniterative scheme for unsteady boundary layer', *AIAA J.*, **16,** 1408–1414 (1981).
8. J. S. Kim and K. S. Chang, 'A noniterative finite difference method for the compressible unsteady laminar boundary layer', *AIAA J.*, **23,** 1826–1828 (1985).
9. J. S. Kim and K. S. Chang, 'Finite difference analysis of unsteady mixed convection on inclined flat plate', *Proc. Fourth Int. Conf. on Numerical Methods in Thermal Problems, Vol. 4*, Swansea, 525–536, 1985.
10. A. J. Robins and J. A. Howarth, 'Boundary layer development at a two-dimensional rear stagnation point', *J. Fluid Mech.*, **56,** 161–171 (1972).
11. J. H. Merkin, 'Mixed convection from a horizontal circular cylinder', *Int. J. Heat Mass Transfer*, **20,** 73–76 (1977).